University of California, San Diego UCSD-CER-06-04

ARIES CS Report: Helium cooled divertor design study

T. Ihli, A. R. Raffray and the ARIES Team

July 2005

Center for Energy Research
University of California, San Diego
9500 Gilman Drive
La Jolla, CA 92093-0420

ARIES-CS Report: Helium cooled divertor design study

T. Ihli[a],A. R. Raffray[b] and the ARIES Team

[a] Forschungszentrum Karlsruhe GmbH, P. O. Box 36 40, 76021 Karlsruhe, Germany

thomas.ihli@imf.fzk.de

[b] University of California, San Diego, 458 EBU-II, 9500 Gilman Dr., La Jolla CA 92093-0438, USA

1 ABSTRACT

With the beginning of Phase II of the ARIES-CS study a major focus of the engineering activities turned towards the conceptual design of the divertor and the divertor physics. As a result of the design approach a new promising divertor concept is presented in this paper. While the concept builds on some basic features from recently presented DEMO related divertor designs [1], a number of decisive new solutions were introduced and specific needs of the compact stellarator divertor in the fields of manifolding and reactor integration were addressed. Major results from the thermo-mechanical analysis are summarized in this contribution and key performance, fabrication and integration issues are discussed.

2 INTRODUCTION

The ARIES-CS compact stellarator study has been launched with the goal of developing through physics and engineering optimization a more attractive power plant concept based on a compact stellarator (CS) configuration. A gas-cooled divertor is envisaged for the ARIES-CS power plant study as the helium cooled, high temperature output (~ 700 °C) divertor type fits very well into the overall plant concept with in-reactor coolant transferring their energy through a heat exchanger to a helium working fluid driving a closed Brayton cycle. The study is focused on a commercial long term fusion power plant and therefore, future extrapolations in the fields of physics and technology are essential whereby the aim is to base on realistic assumptions balanced between optimism and pessimism. In regard on the gas cooled divertor especially a reasonable amount of progress in the fields of materials had to be anticipated during the design approach.

As a key component, the heat exchange structure of a gas cooled divertor is very likely to be built up from a modular arrangement of cooled refractory alloy parts, to handle the peak heat fluxes (assumed as ~10 MW/m² in anticipation of better estimates from the ongoing divertor physics modeling effort). Recently presented near-term design concepts [1] rely on small and simple shaped heat transfer caps (typical diameter between 15 and 20 mm). For a power plant like ARIES CS it was decided to explore a new configuration with suitably increased single part size (relying on anticipated progress in tungsten alloy technologies).

3 TARGET CONCEPT

As an important advantage it is assumed, that no major disruption events will occur in a compact stellarator fusion reactor and from this the requirements on the target's armor layer are less demanding in comparison with near-term tokamaks. In absence of armor melting events due to disruptions the need and thickness of a sacrificial armor layer depend on the sputtering rate resulting from the amount and energy of the different surface hitting particles and the target's material properties. These parameters are not yet determined in detail but it was foreseen that - if necessary - a sacrificial layer made of small segments (likely cuboids) will be brazed onto the directly cooled target structure. It is assumed that the impact of these small cuboids on the stress levels in the structure below is small and from this can be neglected in the current status of the design approach.

Therefore, the focus of the target design development was on the basic target structure made from tungsten alloy and an efficient gas cooling technique which is necessary to keep the structure's temperature within the design limits.

3.1 Basic target structure

The allowable heat load on the critical directly cooled and pressure carrying target structure is restraint by the total stress levels – mainly thermal stresses due to the high heat flux – which have to be kept below the design limits. Reduced thermal stress levels can be achieved by (i) keeping temperature differences small and by (ii) minimizing the restraints against the relative thermal expansions and deformations during heat up. The later requirement can be achieved by segmentation of the target structure in small single parts and by introducing a flexible part design. The temperature differences in the cooled walls are proportional to both the temperature gradient in the wall and the wall thickness. As the temperature gradient is determined as a linear function of the heat flux only the thickness of the cooled walls can be influenced by the design. A small wall thickness for a pressure carrying component can be achieved by a suitable curved shape and a small cooling channel width.

These considerations lead to the development of a target built from small separate T-tubes with the following advantages:

+ Circular cross section and small diameter for a small wall thickness and low radial temperature differences in the tube walls.

+ Fairly unrestraint bending of the tubes by use of T-connectors in the tube's middle position.

To avoid shadowing effects a flat basic armor layer on the heat loaded side of the tubes is used, whereby the minimum thickness of the armor layer was set to 0.3 mm. Additional small armor segments (e.g. small cuboids) can be brazed onto the basic armor layer, to adjust for various requirements, as described before.

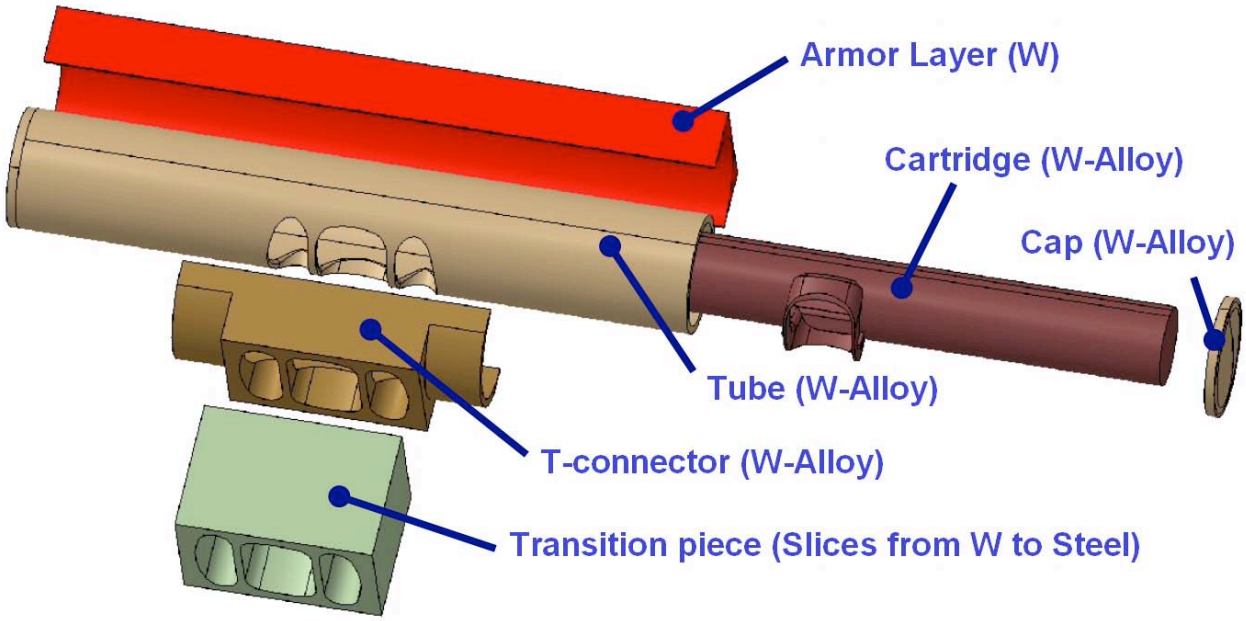

Fig. 1: Design of the T-tube heat exchanger part (explosion view of the CAD model)

Three flow channels are placed in the T-connector and the transition piece, whereby the coolant enters through the middle section and returns through the outer sections. For distribution of the incoming coolant flow within the tubes a concentric cartridge is placed in the tubes, which is connected with the inlet section of the T-connector. To achieve sufficient heat transfer the coolant is accelerated towards the tube's inside by passing a slot in the cartridge (see the cooling technique section). After impingement the coolant returns through the annular gap between tube and cartridge towards the outlet sections in the T-connector.

3.2 Cooling technique

The inside of the tube has to be cooled very effectively to keep the maximum temperature within the tube below the design limit (which was assumed to be about 1300°C due to a starting recrystallization process). From the European HEMJ (or multijet) divertor concept it is known, that a very high heat transfer coefficient can be reached by using the jet impingement cooling technique. This technique can be employed directly due to its simple design involving a plenum

chamber (concentric cartridges in the tubes) and orifices (holes or slots in the cartridges). The outlet velocity of the impinged jets is high enough to result in turbulent flow immediately after impingement. The characteristic coolant flow along the wall inside after impingement (wall jet) is extremely turbulent with high velocity fluctuations and increased local turbulent mixing. As a result, a significant increase in the heat transfer performance is achieved.

An advantage of the proposed T-tube geometry is the large inside of the tubes, which can be used to transfer heat to the coolant. Therefore, the averaged heat transfer coefficient at the upper half of the inside of the tube can be kept relatively low, e.g. 17000 W/m²K for a heat load of 10 MW/m² and an outer tube diameter of 15 mm. As a result of the circular cross section, the highest heat flux occurs in the middle position of the tube and decays towards the sides. From this high heat transfer coefficients are needed in the middle position and decaying heat transfer coefficients towards the sides are favourable to reduce temperature gradients in circumferential direction of the tube. This cooling characteristic can be created by a single longitudinal coolant jet which impinges normal on the inside of the tube at the middle position and than follows sidewise the tube inside as a wall jet flow whereby velocity and turbulence decay with the distance from the impinging region. To create such a normal jet a longitudinal slot at the upper side of the cartridge is used (see fig. 2).

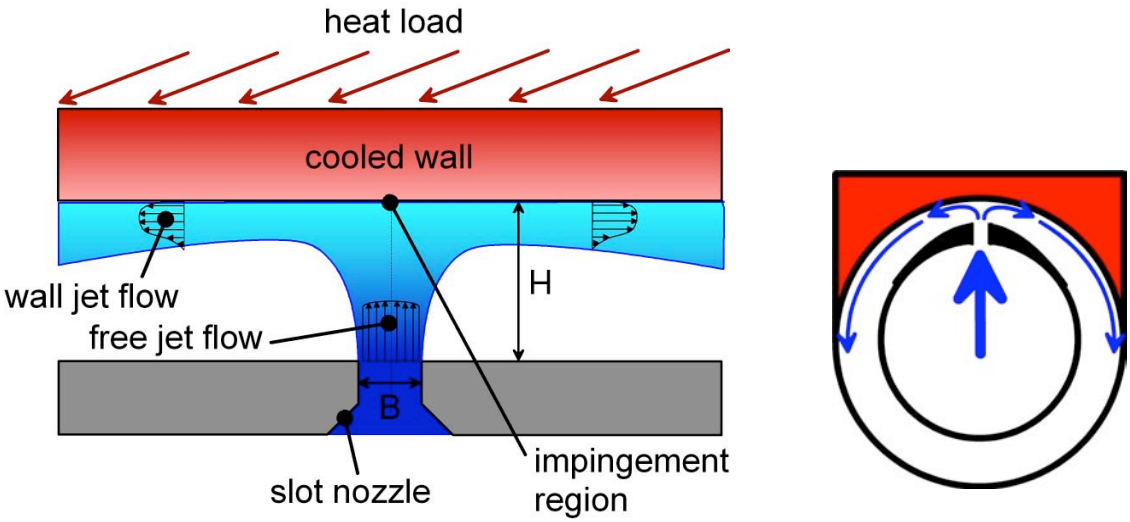

Fig. 2: Slot based jet impingement cooling principle

The coolant mass flow per heat loaded surface area has to be sufficient to keep the coolant temperatures below the design limits of the used structural steel and to allow for sufficient heat transfer capacity. Exemplary layout parameters for the case of a surface heat flux of 10 MW/m² are shown in table 1.

Table 1: basic layout for 10 MW/m²

He pressure		10	MPa
mass flow / heat loaded surface		24	kg/(s m²)
outer diameter of T-tube		15	mm
slot width B		0.5	mm
pressure drop for jet	~	0.07	MPa
tor. tube-tube distance (tube length)		90	mm
poloidal gap between armor		0.2	mm
armor width		15.6	mm
averaged jet velocity	~	200	m/s
averaged heat transfer coefficient	~	17,000	W/m²K
jet-wall distance H		1.25	mm

4 TARGET ANALYSIS

4.1 Design robustness

A reliable cooling system has to be robust against unavoidable geometrical uncertainties and e.g. deformations which might occur during the years of operation. In this respect the described T-tube divertor concept is very promising due to the characteristics of the involved jet cooling system.

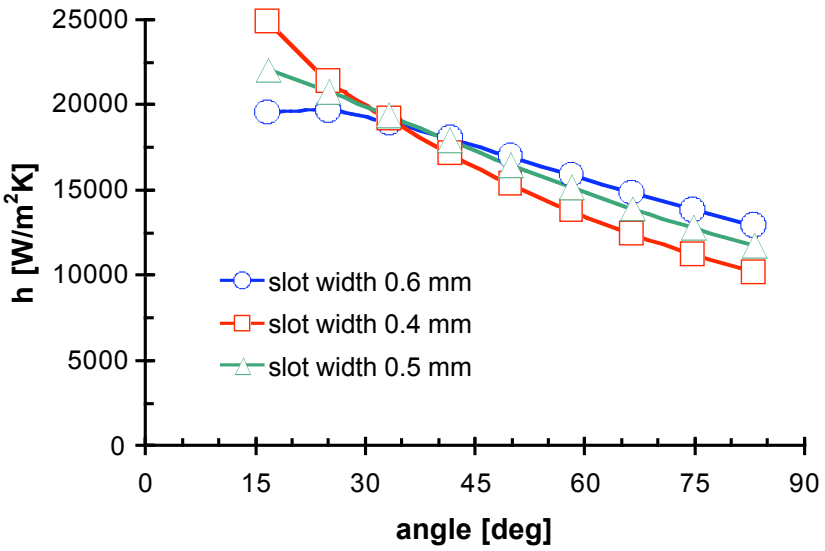

Fig. 3: heat transfer coefficient at the inside of the tube vs. angular distance from impingement point for different slot widths

The influence of the cartridge position in the tube on the cooling performance is very small, as the cooling function is based on wall jet flows which are produced fairly independent from the gap between the cartridge and the outer tube. The slot nozzles are the only flow contraction region within the flow path and as a consequence a dominating fraction of the total pressure drop is available for the acceleration in the slot nozzles. The slot width can be fabricated exactly and does not depend on relative positions between different parts. Nevertheless the cooling system would be robust even against large deviations in the slot width as demonstrated below. In fig. 3 the local heat transfer coefficient determined by use of correlations is plotted versus the angular distance from the middle position in the upper half of the tube (distance from impingement point) for three different slot sizes. It is evident that the overall heat transfer coefficient at the wall inside is only slightly influenced by the slot width, especially at the angular position of 30 degree, where the highest wall temperatures in the tube can be expected. From this it can be stated, that for a given pressure ratio, which is provided and controlled by the circulation system, the heat transfer capacity in the tubes will be very stable and robust against geometrical uncertainties. The coolant mass flow and heat up in the several tubes will vary slightly if some deviations in slot width is assumed, but the total mass flow and total coolant heat up will be a fairly stable averaged value.

4.2 Thermal stress analysis

The Ansys Workbench 9 software package was utilized to calculate the stresses and deformations within the T-tube basic configuration for an internal helium pressure of 10 MPa and a heat load of 10 MW/m². The armor layer is planned to be brazed onto the tube but nevertheless a bonded interface was used between these two parts representing a worst case in terms of stiffness and resulting thermal stress levels. The highest stress levels occur in the T-junction area as the T-connector restrains the free bending of the tube.

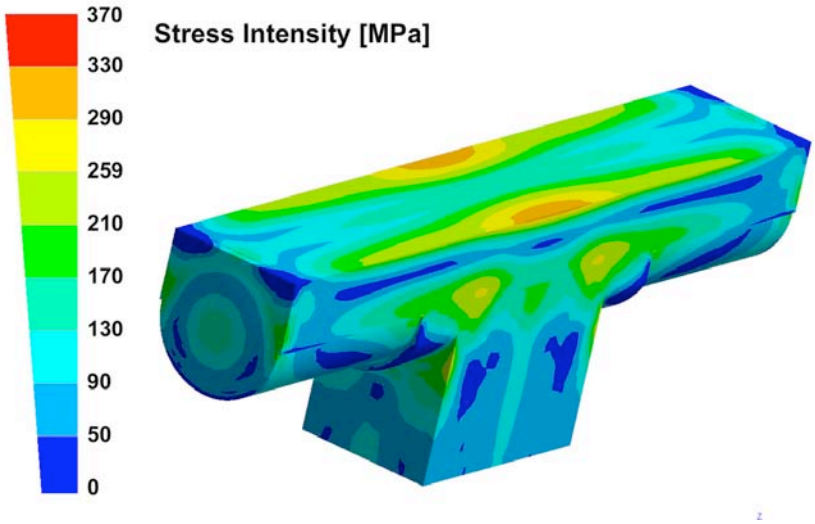

Fig. 4: stress intensity for the basic layout and a surface heat flux of 10 MW/m²

5 MATERIALS & FABRICATION

The directly cooled heat transfer parts of the gas cooled divertor target are made from tungsten alloy. It is well known, that the low temperature ductility and the ductile to brittle transition temperature (DBTT) of a tungsten alloy can be dramatically improved by alloying rhenium. On the basis of first experimental results for irradiated tungsten alloys it seems to be most promising to keep the fraction of Re in the alloy small. For an improved tungsten alloy a DBTT of 600°C and a recrystallization temperature of 1300°C might be a reasonable estimation, which was used as boundary condition for the current design approach. Of course other tungsten material options exist and highly worked materials may provide good properties, especially when used in relatively thin walled and small parts, as considered for the current divertor design.

The main structure of the divertor targets is planned to be made from an advanced ferritic steel like the nano-size particle strengthened grade 12YWT. The assumed maximum operational temperature of such type of steel is in the range of 750°C. Therefore, and to provide some safety margin the maximum coolant temperature was set to 700°C.

The tube and its end caps as well as the T-connector may be produced by plasma spraying or as CVD-tungsten parts. The cartridge is cooled from in- and outside and could therefore be made from a tungsten based material like Densimet 18, which would allow for favorable mechanical machining.

To reduce the thermal stress levels due to different thermal expansion coefficients of ferritic steel and tungsten alloy a graded transition piece is foreseen in the T-junction area of the tubes. The transition pieces could be fabricated as a sandwich of slices from different material grades to adjust step by step in terms of thermal expansion. The slices could possibly be diffusion welded under high isostatic pressure (HIP) utilizing thin brazing foils between each layer to improve the diffusion bonding process.

6 MANIFOLDS & REACTOR INTEGRATION

The T-tubes will be favorably aligned with the magnetic field lines (likely toroidal), whereby supporting manifold modules below the tubes will be directed perpendicular to the tubes. The manifold modules will be combined to form the target plates.

To accommodate for relatively high neutron wall loads for a divertor target in the plasma chamber of a compact stellarator (e.g. 3 MW/m^2) it is favorable to cool the walls of the target's steel structure by use of the cold coolant before the main heat-up in the T-tubes. Therefore, the coolant is first piped through small rectangular flow channels in the walls of the manifolds and than enters an inner flow channel in the middle of the manifolds which is surrounded by the cooled walls. These inner flow channels are divided diagonally in a supply section to feed the T-tubes and a collector section for the returning hot coolant flow.

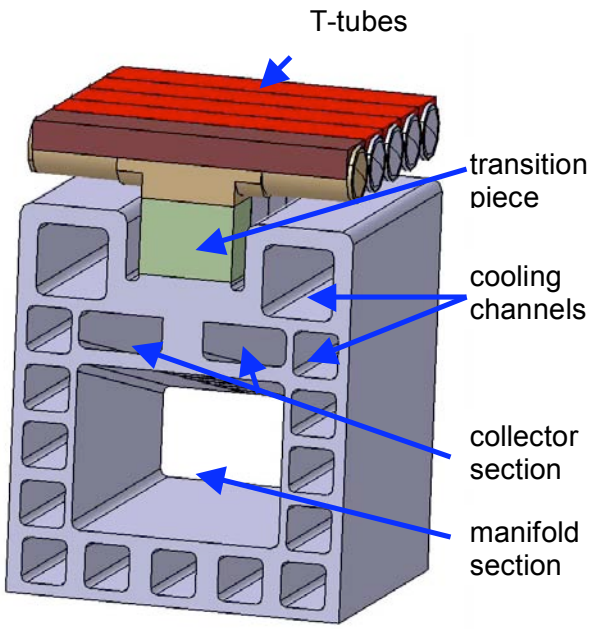

Fig. 5: Target design with T-tubes (tungsten alloy) and Helium cooled manifold (advanced ferritic steel)

7 CONCLUSION

A new design concept for a gas cooled divertor was developed during phase II of the ARIES CS power plant study. The concept is based on a modular arrangement of T-tubes made of tungsten alloy which are acting as Helium cooled target components and heat exchange parts. A slot based jet impingement cooling technique was applied to reach sufficient heat transfer capacity along with reasonable pumping power and pressure drop parameters. The stress levels in the heat loaded geometry are acceptable due to the small wall thickness of the tubes, the high heat conductivity of the used materials and the relatively flexible part design. A new scaling scheme was suggested to adjust the heat exchange parts for various heat flux values. Furthermore new solutions were suggested for the connection of the tungsten components to the steel target manifolds (transition pieces) and a promising target manifold design was presented, which is appropriate even for very high neutron heat loads for targets placed directly in the reactor's main plasma chamber. Different integration schemes were suggested, which can be chosen depending on the available space for the main divertor manifolds, whereby the integration of the divertor main manifolds in blanket boxes results in a particularly space saving and promising arrangement (see appendix).

[1] T. Ihli, et al., An advanced He-cooled divertor concept, SOFT'04, P4C-F228, to appear in Fusion Engineering and Design

Appendix 1: General design and heat transfer concept

A1.1 Design of the heat loaded single part

The basic design involves a divertor target main structure made of an advanced ferritic steel, cooled heat exchanger parts made of tungsten alloy and a segmented tungsten armor layer. An extensive segmentation of the heat loaded target can be reached by use of an array of gas cooled caps, each carrying a separate armor segment as shown in fig. A1.1 (see also [1]).

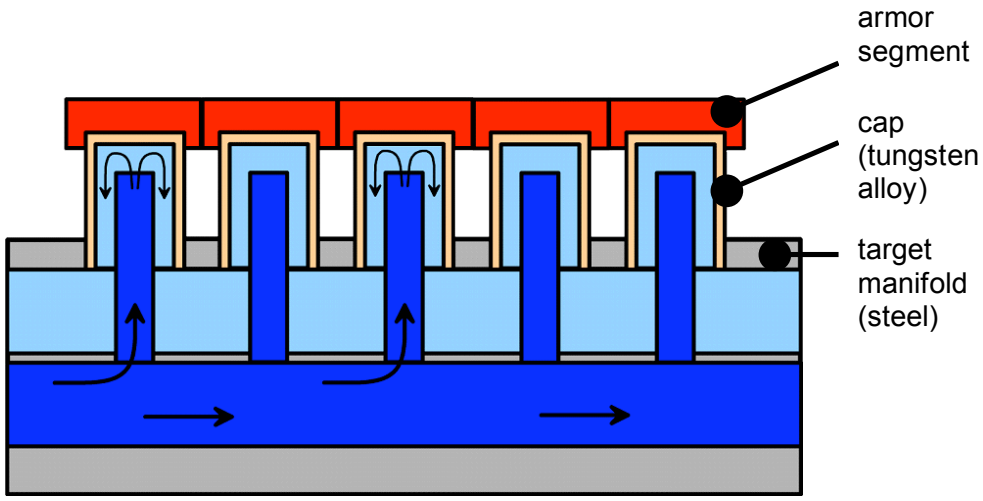

Fig. A1.1: divertor target with tungsten alloy caps and segmented armor layer (schematic)

It was explored how the number of single parts could be reduced without severe drawbacks in terms of thermal stresses (due to a stiffer structure) or larger material transition zones between the refractory alloy single parts and the steel bulk.

As result of a scoping study small tubes made of refractory alloy to be used as heat exchange parts were identified to be a promising alternative geometrical possibility. Tubes with the same diameter as the caps used in forgoing concepts could yield to larger single part sizes. Similar to reasonable curved caps and in contrast to plate designs tubes can be highly pressure loaded without the need of very thick walls. Therefore, it can be assumed that tubes would be reasonable in terms of the wall thickness and flexibility of the parts and from this thermal stress levels could be kept below critical limits. On the other hand a reasonable assembly procedure and part design has to be developed.

The cylindrical heat transfer parts (tube segments) in principle could be arranged in different schemes, but the different thermal expansions between the tubes and the target or main divertor manifolds leads to a geometry option using T-tubes (as shown in fig. A.1.2) which are connected to the target manifolds. Due to the small steel-tungsten connection area the design of the target manifolds is less restraint as for the cap-design shown in fig. A1.1. Further on T-tubes can be tested without the need of pressure resistant sub-modules (e.g. 9 finger modules) as developed for the cap-design [1].

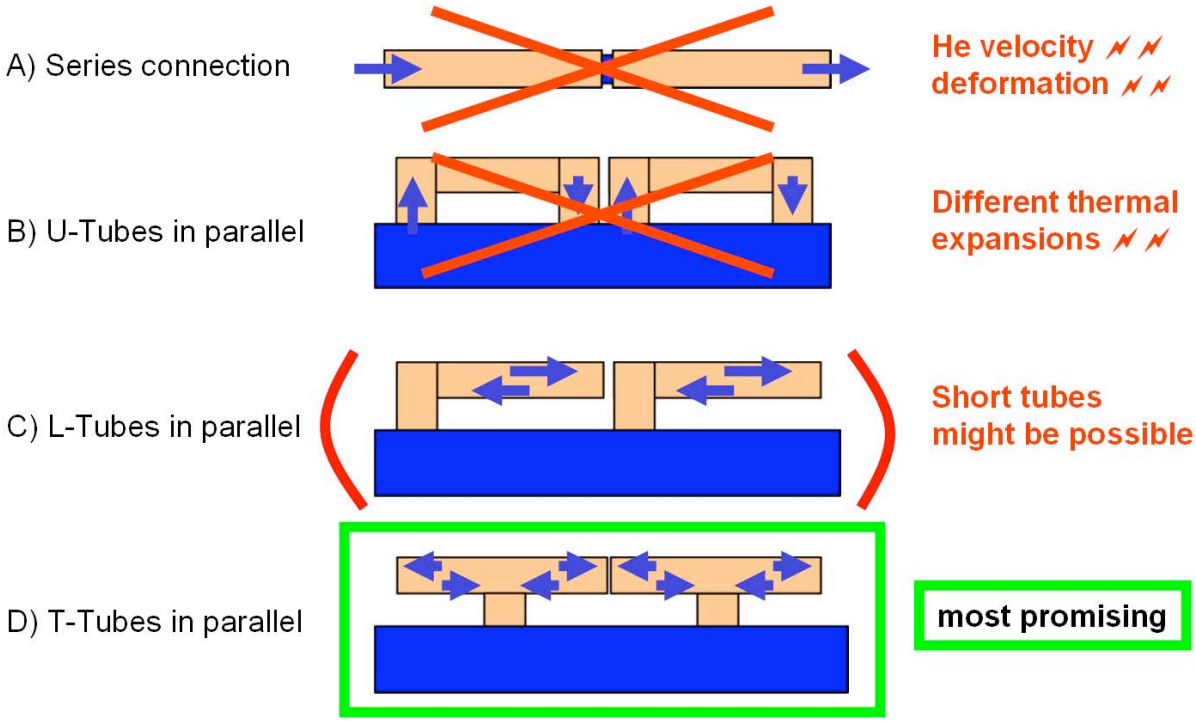

Fig. A1.2: tube-segment options
(schematic: tungsten alloy tubes – beige, steel target manifold - blue)

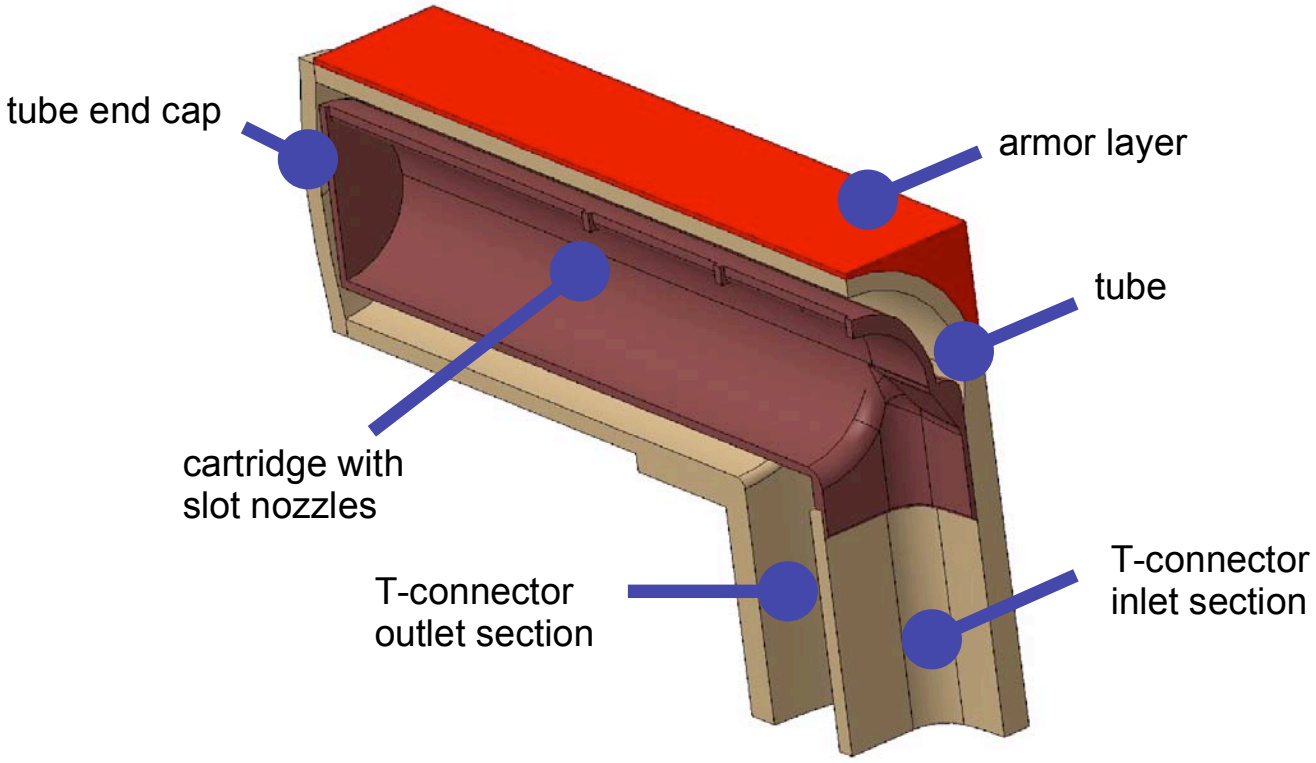

Fig. A1.3: quarter of the CAD model of the T-tube heat exchange part

The detailed CAD Design for the T-tube geometry is illustrated in fig. 1 (explosion drawing) in the main text and in fig. A1.3 showing a quarter of the CAD model, while the dimensions at a cross section of the tube configuration are shown in fig. A1.4

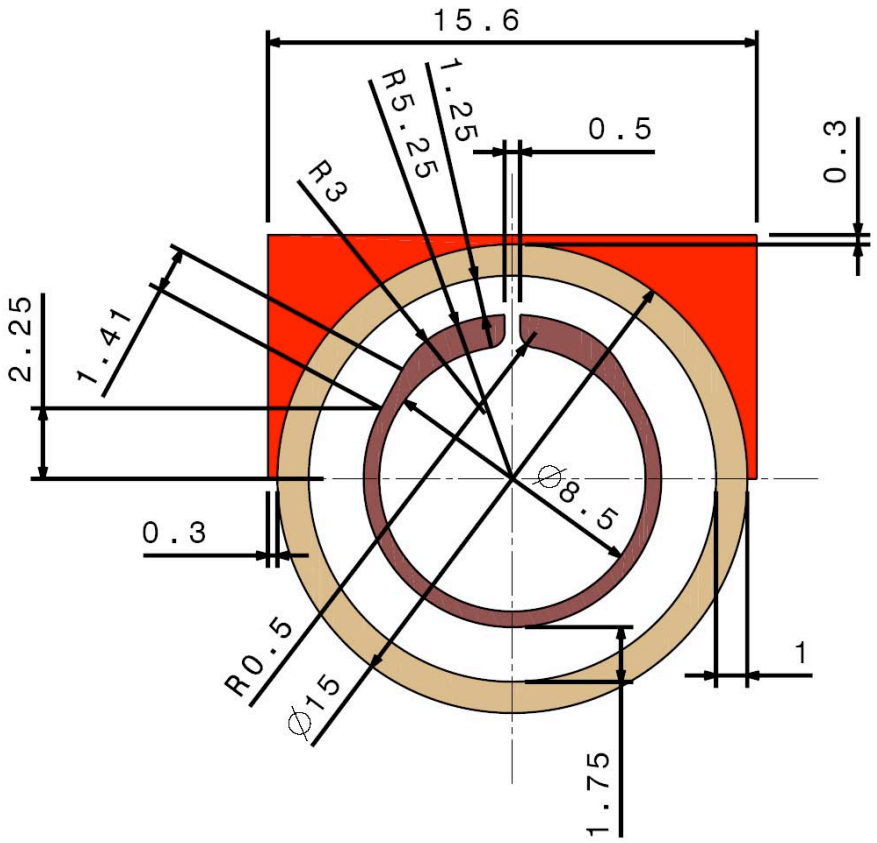

Fig. A1.4: Dimensions at cross section of the T-tube heat exchange part

A1.2 Jet impingement cooling technique

As described in the main text, the slot based jet impingement cooling technique was chosen as a heat transfer enhancement technique for the T-tube heat exchange parts. In comparison to the multiple jet impingement used to cool the caps in the foregoing tokamak divertor design, the averaged heat transfer coefficient is reduced in the current design assuming the same pumping power available for the divertor. But nevertheless due to the larger inner heat transfer surface in the tubes in comparison to the caps the resulting heat transfer coefficient is still sufficient to reach a comparable blower power and pressure drop. Both jet cooling techniques are shown in principle in fig. A1.5.

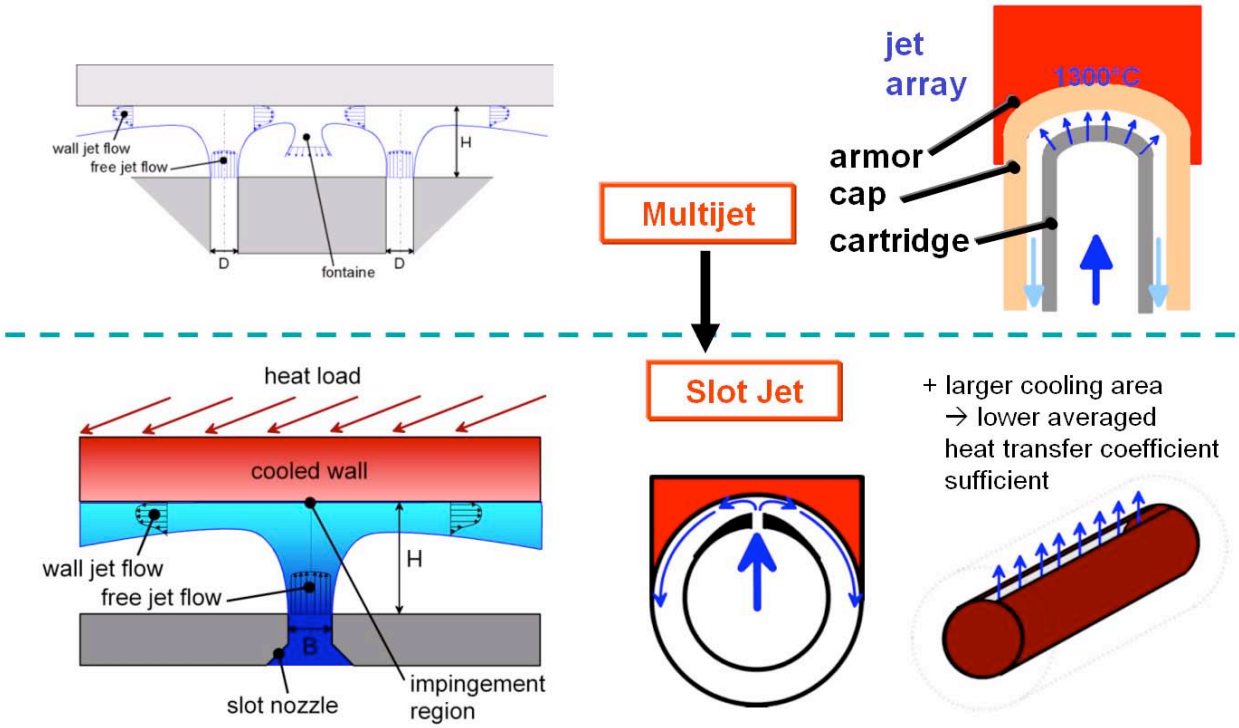

Fig. A1.5: Comparison of multiple drilling and single slot jet impingement cooling

For the preliminary cooling system layout a correlation from the German VDI Waermeatlas was used to estimate the heat transfer in the current geometry and to determine the necessary parameters like slot width and pressure drop between cartridge in- and outside.

Nomenclature:

T_jet	jet temperature (inlet)
T_w	wall temperature
T_m	mean temperature, T_m = (T_jet + T_wall)/2
B	slot width
L	slot length
D	hydraulic diameter, D = 2*B
X	distance from jet centerline along the wall
H	jet-wall spacing
X_nd	nondimensional distance from jet centerline, X_nd = X / D
H_nd	nondimensional jet-wall spacing, H_nd = H / D
□	density
□	viscosity
k	conductivity
c_p	specific heat
G	mass flow through slot

w	averaged jet velocity, w = G/(B*L*)□ (for T_m)
Re	Reynolds number
Pr	Prandtl number
Nu	Nusselt number
h	heat transfer coefficient
m	geometry dependent exponent

NOTE: All gas properties have to be taken for the mean temperature T_m

Common heat transfer equations to be used along with the correlations:

- $\mathrm{Re} = \frac{D \cdot w \cdot \rho}{\mu}$
- $\mathrm{Pr} = \frac{\mu \cdot c_p}{k}$
- $h = \frac{Nu}{D \cdot k}$

Correlation:

- $m = 0.695 - \frac{1}{X_{nd} + H_{nd}^{1.33} + 3.06}$
- averaged Nusselt number in the area between jet center and X:

$$Nu = \frac{1.53 \cdot \mathrm{Re}^m \cdot \mathrm{Pr}^{0.42}}{\left(X_{nd} + H_{nd} + 1.39\right)}$$

The following layout was assumed to be sufficient to fulfill the materials boundary condition (T_{max} = 1300°C) with a He-inlet temperature of 600°C at a pressure of 10 MPa:

B = 0.5 mm, H = 1.2 mm, R_i = 6.5 mm ($X = \pi \cdot R_i$)

In fig. A1.6 the heat transfer coefficients obtained for different layout examples are shown together. The layout examples correspond to different heat load cases and tube sizes as indicated by the data in the boxes according to the different curves.

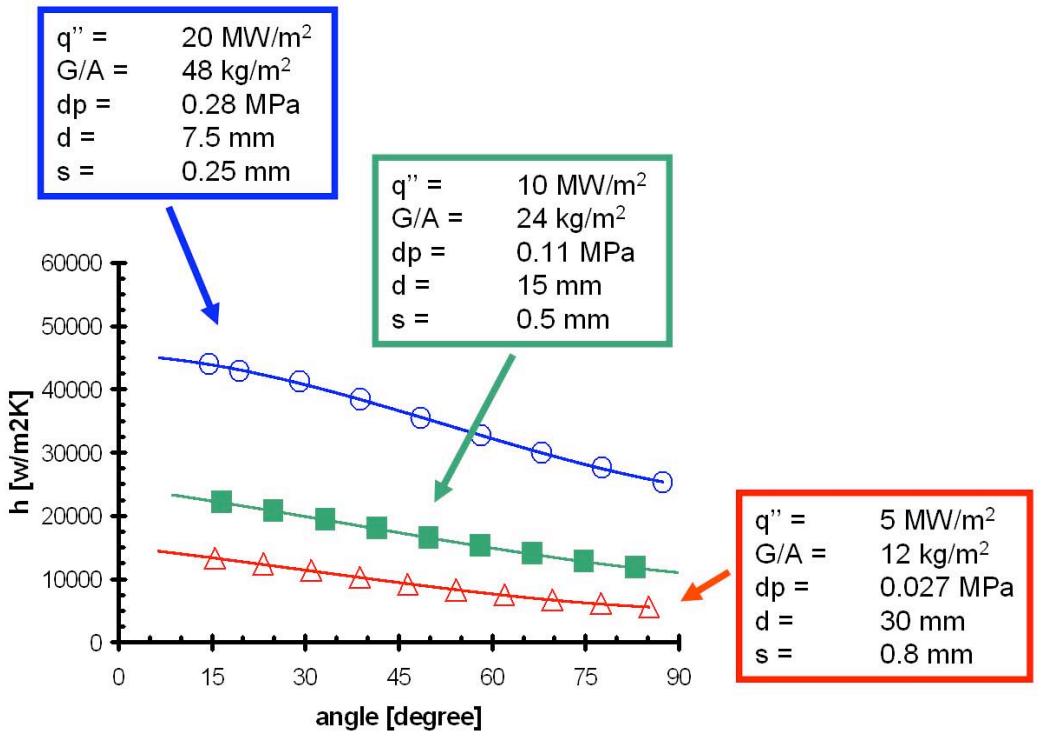

Fig. A1.6: heat transfer coefficients vs. angular position (zero at mid-plane) for different heat fluxes and layout cases

Note: The correlation used in fig. A1.6 cannot resolve the main impingement region (approximately 0 to 10 degrees). For this region additional CFD calculation showed that the heat transfer coefficient can be as high as 50,000 W/m²K for the 10 MW/m² heat flux layout case (see green box and green curve in diagram A1.6).

Appendix 2: Detailed structural and thermal study

A2.1 Preliminary layout of the T-Tubes

To evaluate a reasonable start value for the dimension of the small heat exchanger parts, namely the T-tube's diameter, an estimation effort was applied (see sub-section A2.1.1). The estimation was based on the assumption of the T-tubes being a rather flexible structure whereby the stress levels within the upper heat loaded side of the tube are determined by the upper side's total wall thickness (tube + armor) and the heat flux through the upper side. As the influence of the tube shape, the T-connector and the lower tube side are neglected (all of these may cause stiffening effects) the determined allowable tube diameter will presumably represent an upper limit. A stress formula for an extended heat loaded and unrestrained bending plate was applied to the problem of the heat loaded and bending T-tubes.

In contrast - as described in sub-section A2.1.2 - an estimation based on a circumferentially uniform heat loaded and internally cooled tube doesn't provide realistic stress values, as the essential stress reduction due to the bending of the tube (flexibility) is not considered in this load case.

A2.1.1 Estimation of the allowable tube diameter (by relating to stresses in a bending heat loaded plate)

The stresses in a plate under heat load are a function of the temperature gradient in the heat loaded wall dT/ds (which is determined by the heat flux and the material's thermal conductivity k), the Young's modulus E, the wall thickness s and the thermal expansion coefficient $\square$ (see equation (A2.1)). In accordance with a common layout rule for concrete road plates [A2.1], the maximum stress level within a heat loaded plate (free bending assumed) can be calculated:

$$\sigma_W = \frac{s \cdot \frac{dT}{ds} \cdot \alpha \cdot E}{2} \qquad \text{with } \frac{dT}{ds} = \frac{\dot{q}}{k}, \ (\dot{q} \text{ - heat flux}) \tag{A2.1}$$

[A2.1] Eisenmann, J., Messungen an Versuchsstrecken bei Betonstrassen 1967, Strasse und Autobahn H. 12, S. 418, 0656

To transfer the equation for the bending stress (A2.1) to the current case of a tube with flat armor layer on its top it might be a reasonable first approximation to use as a plate thickness the averaged thickness of the material above the inside of the upper half of the tube (addition of tube wall thickness and the thin flat armor layer on the tube's upper side as described before and illustrated in fig. A1.4). In the following this averaged wall thickness on the heat loaded side is estimated starting with the cross section A of the material in one half of the upper tube side whereby R is the distance from the tube center to the top of the armor (same as distance form the center to the side of the armor) and s_{tube} is the material thickness in the center of the armor (same as minimum material thickness at the sides of the upper half of the tube):

(A2.2) $$A = R^2 - \frac{\pi}{4}\cdot\left(R - R\cdot\frac{s_{tube}}{R}\right)^2 = R^2\cdot\left(1 - \frac{\pi}{4}\cdot\left(1 - \frac{s_{tube}}{R}\right)^2\right)$$

The averaged wall thickness (s = A/R) than can be calculated as follows:

(A2.3) $$s = R\cdot\left(1 - \frac{\partial}{4}\cdot\left(1 - \frac{s_{tube}}{R}\right)^2\right)$$

In accordance with fig. A1.4 we set $\frac{s_{tube}}{R}$=1.3/7.8, this and equation (A2.3) results in:

s = 0.454 * R = 0.227 * D

Using this relation between the wall thickness and the outer tube diameter along with equation (A2.1) and additional correction factors *f1* and *f2* to adjust for the non-uniformity of the heat flux across the tube's wall (explanation see below) the maximum allowed diameter of the tube can be calculated to be:

(A2.4) $$D_{\max} = \frac{6\cdot Sm\cdot k}{0.227\cdot\alpha\cdot E\cdot f_1\cdot f_2\cdot\dot{q}} \approx 0.0185m = 18.5mm,$$

with: Sm = 350/3 MPa
k = 100 W/mK
□ = 4.6e-6
E = 400 GPa
$\dot{q}$ = 10 MW/m²

$$f_1 = \frac{2}{1+\left(\frac{A_{hot}}{A_{cooled}}\right)^{-1}} = \frac{4}{2+\pi\cdot\left(1-\frac{s_{tube}}{R}\right)} = 0.87$$

(f_1 – factor to account for reduced heat flux due to armor top/tube inside surface ratio)

f_2 = 15.8*87.9/(15.6*85) = 1.047

(f_2 – factor to account for higher than nominal heat flux at armor top due to gaps between different heat exchanger parts)

The inner tube diameter is $D_{in} = D_{max}$ (1-1.3/7.8) = 15.4 mm, and the averaged wall thickness as defined above becomes s = 4.2 mm.

Notes:

- Without taking the heat flux correction factors *f1* and *f2* into account the maximum diameter would be calculated to be 16.8 mm.

- By use of detailed 3D finite element stress calculations for the real geometry with all stiffening effects being taken into account and with the additional internal tube pressure of 10 MPa, a reasonable inner diameter for the tube was determined to be 13 mm (and 15.6 mm at the tube's outside = inner tube diameter + 2 * wall thickness of 1 mm + 2 * minimum armor thickness of 0.3 mm) for a heat flux of 10 MW/m². In this case the averaged upper wall thickness taking the complete armor layer into account is 3.54 mm (see fig. A1.4).

A2.1.2 Estimation of thermal stresses for an uniformly heat loaded and cooled cylinder

The thermal stresses at the inside of a circumferentially uniform heat loaded (in- or outside) and cooled cylinder (other side) can be calculated:

(A2.5) $$\sigma_W = \frac{\Delta T \cdot \alpha \cdot E}{2 \cdot (1-\nu) \cdot \ln\left(\frac{R_{out}}{R_{in}}\right)} \cdot \left(1 - \frac{2 \cdot {R_{out}}^2}{{R_{out}}^2 - {R_{in}}^2} \cdot \ln\left(\frac{R_{out}}{R_{in}}\right)\right)$$

[A2.2] W.C. Young and R. G. Budynas, Roark's formula for stress and strain, McGraw-Hill, 7th ed. p. 762

With the above described correction terms (see section A.2.1.1) for the heat flux across the tube wall:

(A2.6) $$\sigma_W \approx \frac{s \cdot \alpha \cdot E \cdot \dot{q} \cdot f_1 \cdot f_2}{k \cdot 2 \cdot (1-\nu) \cdot \ln\left(\frac{R_{out}}{R_{in}}\right)} \cdot \left(1 - \frac{2 \cdot {R_{out}}^2}{{R_{out}}^2 - {R_{in}}^2} \cdot \ln\left(\frac{R_{out}}{R_{in}}\right)\right)$$

With the boundary conditions listed above and $s = R_{out} - R_{in}$ = 3.54 mm and R_{in} = 6.5 mm the tensile stress at the inside of the cylinder using the equation A2.6 can be calculated to be in the range of 480 MPa. From this the estimated stress level is above the numerically calculated stress level for the real geometry (result from FE analysis: 370 MPa), which is likely to be due to the fact, that the real geometry is heat loaded only at one side and is appropriate to bend what reduces the thermal stresses in the tube. The first estimation (sub-section A2.1.1) seems to be more appropriate for the current case of a relative flexible geometry, which is heat loaded only at one side.

The equations (A2.1) and (A2.5) indicate, that in both cases (estimation A2.1.1 and A2.1.2) the stress level stays constant, if the geometry is scaled up in all coordinate directions while the heat flux is reduced anti proportional to the scaling ratio s_f:

$$\dot{q} \sim \frac{1}{s_f}$$

Also stress calculations (FE analyses) indicated, that the scaling of the geometry in accordance with the heat load as shown above results in constant maximum stress intensities within the T-tube geometry. This dependency can be used to adjust the geometry for various heat flux conditions (for details turn to section A2.2.1).

A2.2 Adjustment of jet cooled T-tube heat exchanger geometry to various heat loads

A2.2.1 Scaling of T-tube geometry and relative mass flow

As for constant stress levels the diameter and dimension of the T-tubes in first approximation has to be reduced linearly with increasing heat flux (see chapter A2.1.1), it is proposed here, to scale the geometry (in all three coordinates) linearly with the inverse heat flux ratio (in regard on the basic layout for 10 MW/m²), whereby s_f is the geometry scaling factor:

$$s_f \sim \frac{1}{\dot{q}}$$

It can be shown, that in first approximation the requirement for constant maximum temperatures in the tube walls,

$$\dot{q} \sim h$$

is fulfilled, if the mass flow per heat loaded unit is adjusted linearly with the heat flux:

$$\frac{\dot{m}}{A_{hot}} \sim \dot{q} \sim \frac{1}{s_f}$$

For the jet velocity w this results in: $w \sim \frac{1}{s_f}$

It can be shown that the Reynolds number *Re* is independent from the heat flux for the chosen scaling procedure:

$$\mathrm{Re} = \frac{D \cdot w \cdot \rho}{\mu} = D \cdot w \cdot const \sim \frac{1}{s_f} s_f \Rightarrow \mathrm{Re} \neq f(\dot{q})$$

As the Nusselt number *Nu* is a function of non-dimensional geometry factors (constant) and the Reynolds number it is also independent of the heat flux $\dot{q}$. Therefore, it can be shown that the heat transfer coefficient h for jet cooling is proportional to the heat flux for the chosen scaling procedure:

$$h = \frac{Nu}{D \cdot k} \sim \frac{1}{s_f} \sim \dot{q}$$

Further on it can be determined that the pressure drop is proportional to the square of the heat flux:

$$\Delta p \sim w^2 \sim \dot{q}^2$$

Also the local relative pumping power (ratio of blower power and layout heat flux) is proportional to the square of the heat flux as shown below.

$$\frac{P}{\dot{Q}} \sim \frac{\dot{m}}{A}\Delta p \cdot \frac{1}{\dot{q}} \sim \dot{q} \cdot \dot{q}^2 \cdot \frac{1}{\dot{q}} = \dot{q}^2$$

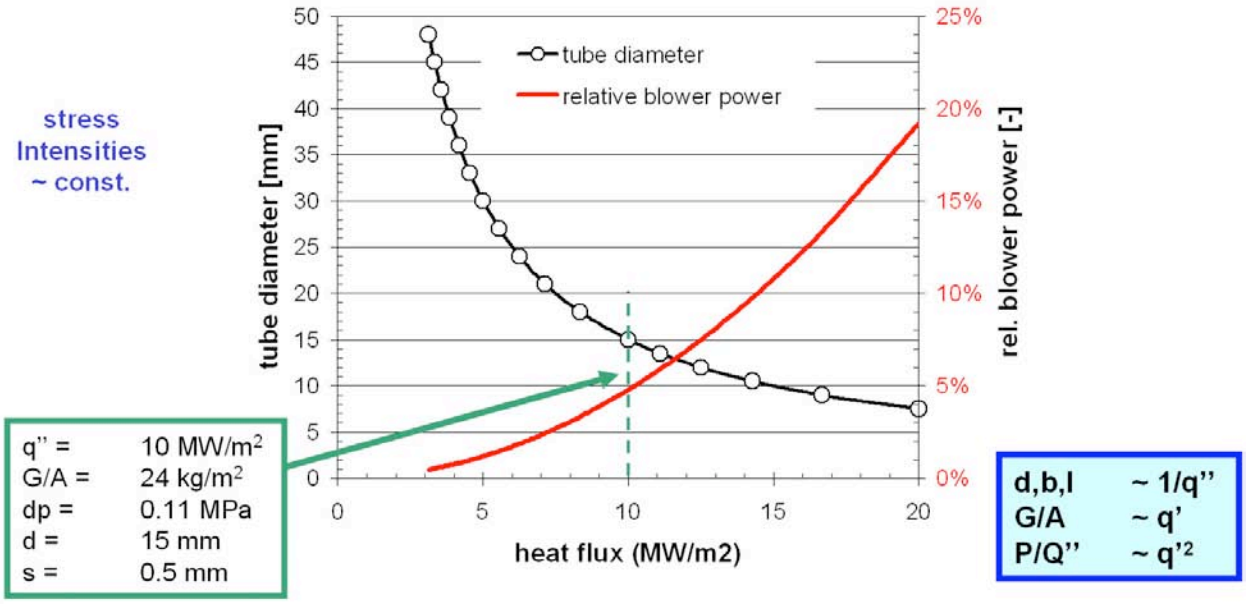

Fig. A2.1: scaled tube diameter and relative blower power vs. heat flux

A2.2.2 Adjustment for lower heat flux without scaling

For a given geometry and size, which is appropriate for a concrete heat flux value due to the range of the occurring thermal stresses, without changing the geometry only an adjustment of the cooling system parameter in the direction of reduced heat flux values is reasonable. The different possibilities for an adjustment without modifying the design of the outer tube/heat exchanger part are discussed below.

For slot based jet impingement the dependency of the Nusselt number from the Reynolds number and the mass flow are:

$$Nu \sim \mathrm{Re}^m \sim \dot{m}^m \approx \dot{m}^{0.6}$$

a) Under the assumption of unchanged material temperatures the heat transfer coefficient should depend linearly on the heat flux ($\dot{q} \sim$ h) and it comes:

$$\dot{q} \sim \dot{m}^{0.6} \Rightarrow \dot{m} \sim \dot{q}^{\frac{5}{3}}$$

with the common dependency $\dot{m} \sim \Delta p^{\frac{1}{2}}$ it comes:

$$\Delta p \sim \dot{q}^{\frac{10}{3}}$$

and for the local relative pumping power:

$$\frac{P}{\dot{Q}} \sim \frac{\dot{m}}{A} \Delta p \cdot \frac{1}{\dot{q}} \sim \dot{q}^{\frac{5}{3}} \cdot \dot{q}^{\frac{10}{3}} \cdot \dot{q}^{-1} = \dot{q}^4$$

As demonstrated in this case the relative pumping power is proportional to the fourth power of the heat flux. As a drawback of the current adjustment procedure the coolant heating *dT* within the heat exchanger parts depends on the heat flux and increases with decreasing heat flux, which may result in exceeding the allowable material temperatures for the steel parts of the divertor.

b) From this the alternative assumption

$$\frac{\dot{m}}{A_{hot}} \sim \dot{q}$$

might be used more frequently, which results in unchanged coolant heating *dT* within the heat transfer component for variable heat loads. Without changing the slot dimension this leads to:

$\Delta p \sim \dot{q}^2$ (same result as for scaled geometry)

For the relative pumping power it comes:

$$\frac{P}{\dot{Q}} \sim \frac{\dot{m}}{A} \Delta p \cdot \frac{1}{\dot{q}} \sim \dot{q} \cdot \dot{q}^2 \cdot \dot{q}^{-1} = \dot{q}^2$$

c)

The same case as shown in sub-section b, but with adjustment of the slot dimension (larger slot for reduced heat flux) leads to reduced pumping power in contrast to the foregoing case, but also to a declined ratio of slot pressure drop versus tube pressure drop and therefore reduced accuracy in mass balancing. The pumping power for case c) can't be given as a simple function, but it might be stated, that it may range between the pressure drops for cases a) and b).

A2.3 Asymmetric heat load

An asymmetric heat load on a heat exchanger part could occur during the start of operation, due to some shadowing effects. In later states these effects may be reduced due to sputtering of armor material. For a worst case study (figs. A2.3 and A2.4) the heat load at a limited section of the tube was set to 0 MW/m² and the heat load in the remaining section was set to be 12

MW/m². As a result it could be shown, that no local stress peaks occur in the tube, which indicates that the geometry is robust against asymmetric heat load.

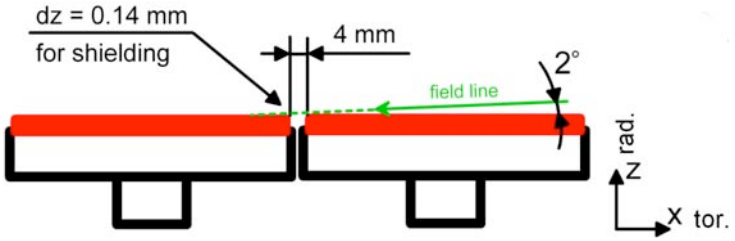

Fig. A2.2: exemplary field line angle and resulting geometrical parameter

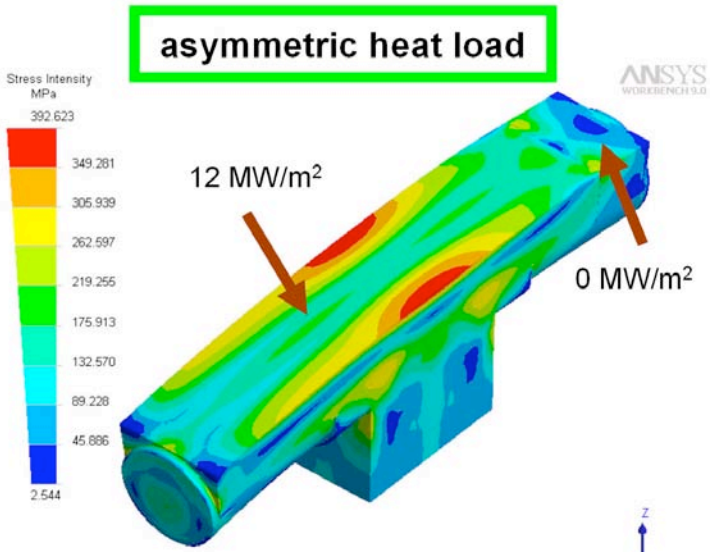

Fig. A2.3: primary and secondary stress intensity for asymmetric heat load

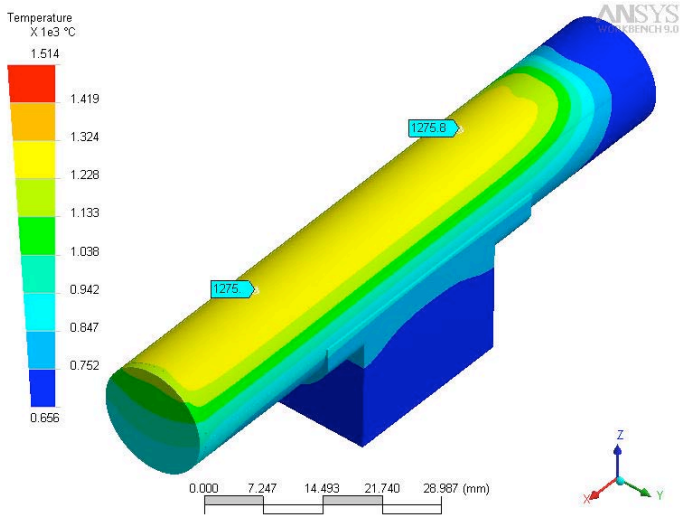

Fig. A2.4: outside temperature distribution of cooled tube for asymmetric heat load

A2.3 Heat loaded ends of the tubes (caps)

It was analyzed if the heat load on the tube ends (caps) would result in stress or temperature peaks for the tubes. Results for two cases are shown in picture A2.5, whereby on the left side the heat load on the tube ends was 10 MW/m² (100% of the heat load in the remaining armor region) and on the right side the heat load on the tube ends was set to be 5 MW/m² (50 % of overall heat flux). In the later case both, temperatures and stress intensities at the tube ends stay below the maxima in the remaining geometry. In the first case the stress intensity at the tube end is in the same range as in the T-connection area, but the temperature at the tube end is slightly higher than in the remaining part of the tube. From this it could be concluded that shielding of the tube ends as indicated in Fig. A2.2 would be favorable, but nevertheless a heat load of at least 50% of the overall heat load at the tube ends wouldn't cause any stress or temperature peaks. This is important as a high fraction of radiated energy result in significant heat load for the tube ends, even if there is a large geometrical step in the armor layer to avoid particle hitting the tube ends.

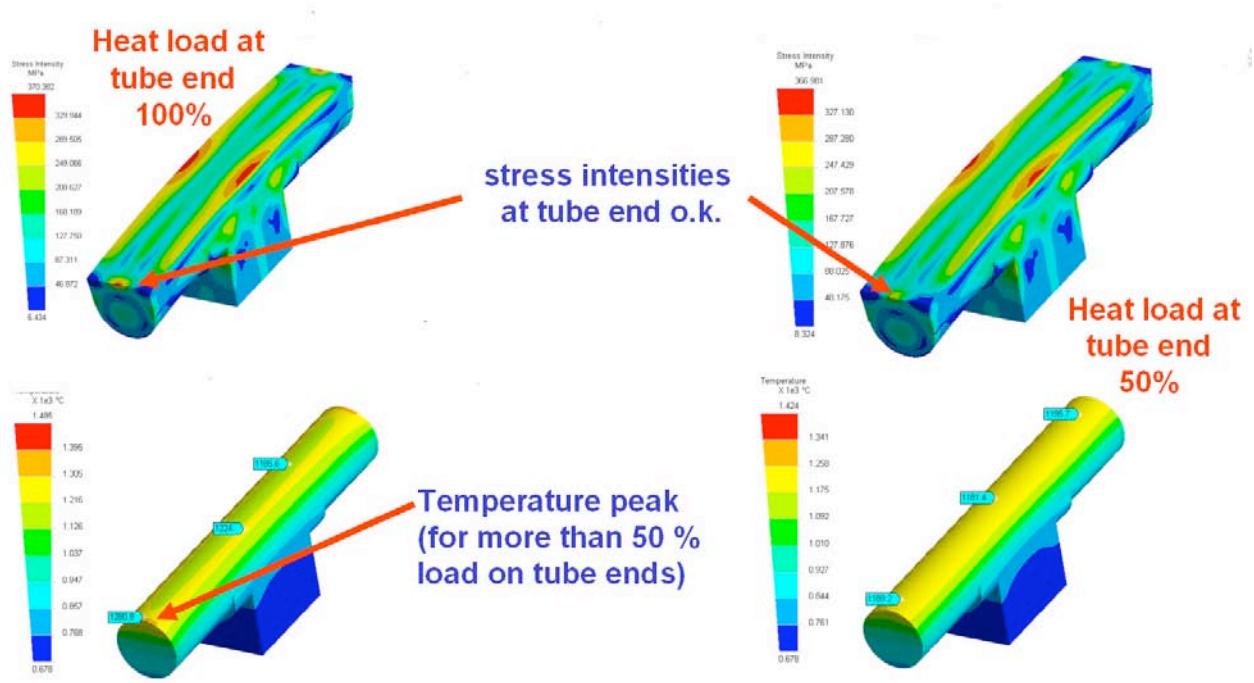

Fig. A2.5: Stress intensities and temperatures for heat loaded tube ends
(left side 100 %, right side 50% of overall surface heat load of 10 MW/m2)

A2.3 W-Fe transition

The connection between the T-tube and the steel manifolds could possibly be made by use of a graded transition zone as indicated in Fig. 2.6. Thermal stress analyses showed, that the stress levels in the transition zone can be drastically reduced even if the transition zone is not made continues but is build from thin plates dealing with increasing thermal expansion coefficients in

direction to the steel manifold. This method results in a stepwise adjustment of the thermal expansion coefficient whereby the number and thickness of the layers could be varied to fulfill the requirements. It is evident that material and fabrication technologies have to be developed to realize the proposed tungsten steel transition zone. The single parts could possibly be brazed in one or few steps under high pressure and temperature to utilize diffusion bonding processes for a strong connection of the layers.

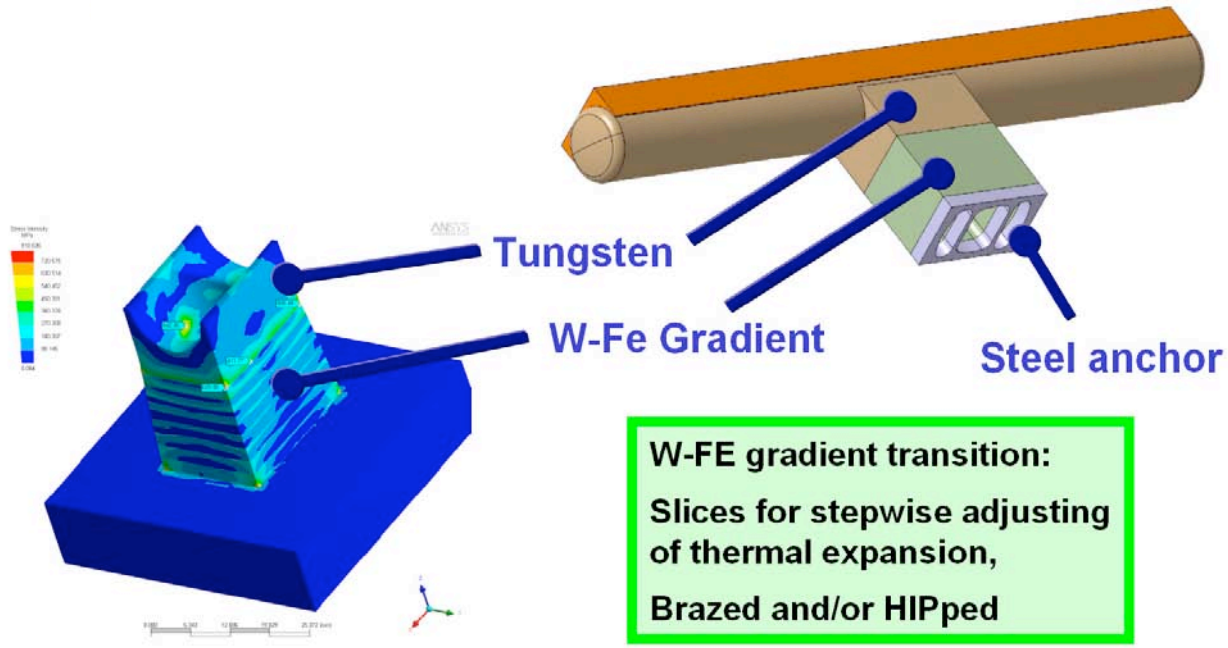

Fig. A2.6: W-FE gradient transition zone for connection of tubes and manifolds

Appendix 3: Target Manifold Design

A3.1 Target manifold design principle

The targets of the divertor in the considered compact stellarator are placed directly in the plasma chamber. Therefore, the neutronic surface power flux tends to be higher as for the vertical targets in the private heat flux region of a typical tokamak configuration. From this the focus has to be turned towards the temperature distribution in the target manifolds due to the volumetric heating. To address the requirements, the target manifold consists of outer cooling channels and the inner main manifold and collector sections. The wall between the manifold and collector section is diagonal to keep the flow velocities nearly constant along the manifolds main direction (likely poloidal, see fig. A3.1). A target stripe module - depending on heat load distribution and peaking factor - may consist of several sub modules which are connected in series (2 sub-modules are shown on the left side of fig. A3.1).

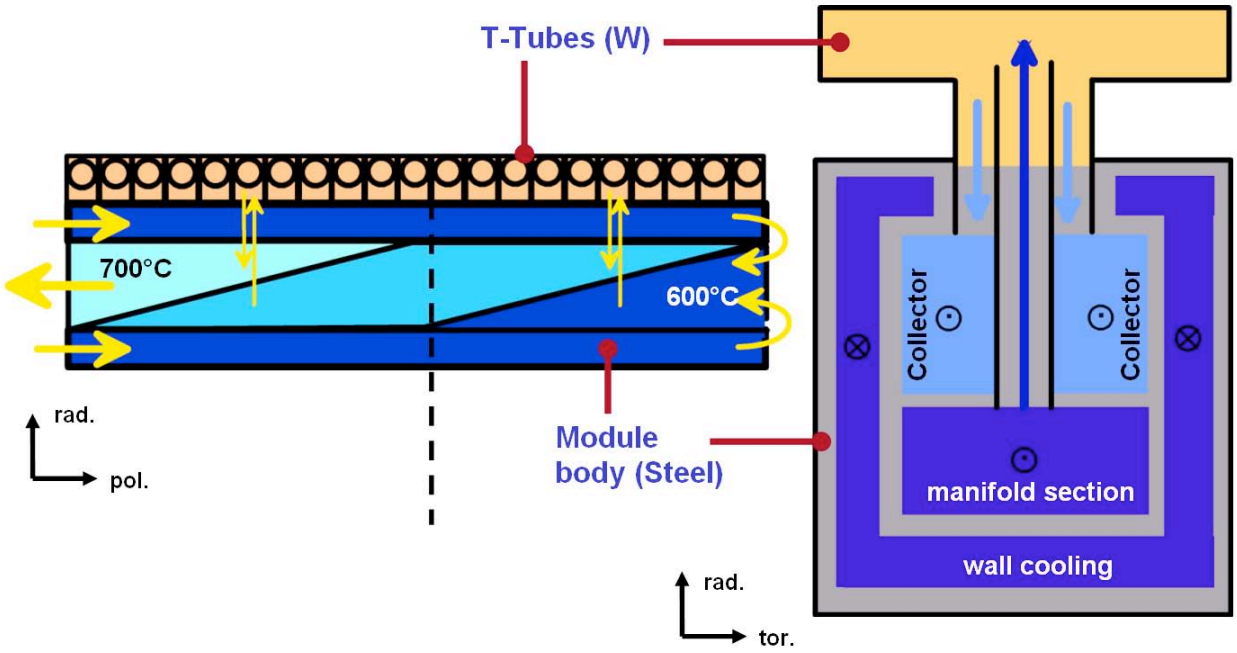

Fig. A3.1: Target manifold design principle

The un-preheated coolant enters the outer cooling channels at a temperature below 600°C. At the end of the stripe modules the flow is turned in the manifold-section of the module (see fig. A3.1) at a temperature of approximately 600°C. From this each T-tube within the first sub-module is fed with coolant of roughly the same inlet temperature and the T-tubes within the next sub-modules are fed by the returning flow coming from the previous sub-module. Therefore the collector section of the previous sub-module is connected to the manifold section of the next sub-module. The layout of the stripe modules and its sub-modules due to local heat flux peaking is likely to be much more complicated for a compact stellarator divertor as for a tokamak divertor. The exact layout will be done when the heat flux distribution functions and geometrical data of

the divertor targets for the ARIES CS reactor will be available as a result from the divertor physics studies. An exemplary layout example will be given in the A4.2 section of this report.

A3.2 Detailed target manifold design

The detailed CAD design of the divertor target manifolds is illustrated in fig. A3.1. The total target radial build consists of three zones, zone 1 being the tungsten only zone, zone two is the transition zone including the transition piece as described in section A2.3 and the main steel bulk zone (zone three) of the target manifold as described in section A3.1. The according volumetric heating rates due to a neutronic surface power load of 3 MW/m² are shown in table A3.1 along with the dimensions of the three zones and the volumetric material fractions.

zone1: Tungsten parts, h = 17.8 mm				NWL: 3 MW/m2	
	Volume per 15.8 mm strip length	fraction of volume	effective radial build	volumetric heating tungsten	volumetric heating steel
	m³	%	mm	MW/m³	MW/m³
sum W	9.540E-06	37.69%	6.71	53.05	
Helium	1.07E-05	42.27%	7.52		
space	5.07E-06	20.04%	3.57		
total	2.53E-05		17.80		
zone2: W-FS-Gradient zone, h = 20 mm					
sum W	1.919E-06	6.75%	1.35	50.00	
sum FS	9.909E-06	34.84%	6.97		23.22
Helium	1.05E-05	36.96%	7.39		
space	6.10E-06	21.45%	4.29		
total	2.84E-05		20.00		
zone3: Manifolds, h = 87 mm					
sum FS	4.00E-05	32.34%	28.13		20.35 ... 14.88
Helium	8.35E-05	67.50%	58.72		
space	2.08E-07	0.17%	0.15		
total	1.24E-04		87.00		

Tab. A3.1: Radial build and volumetric heating data

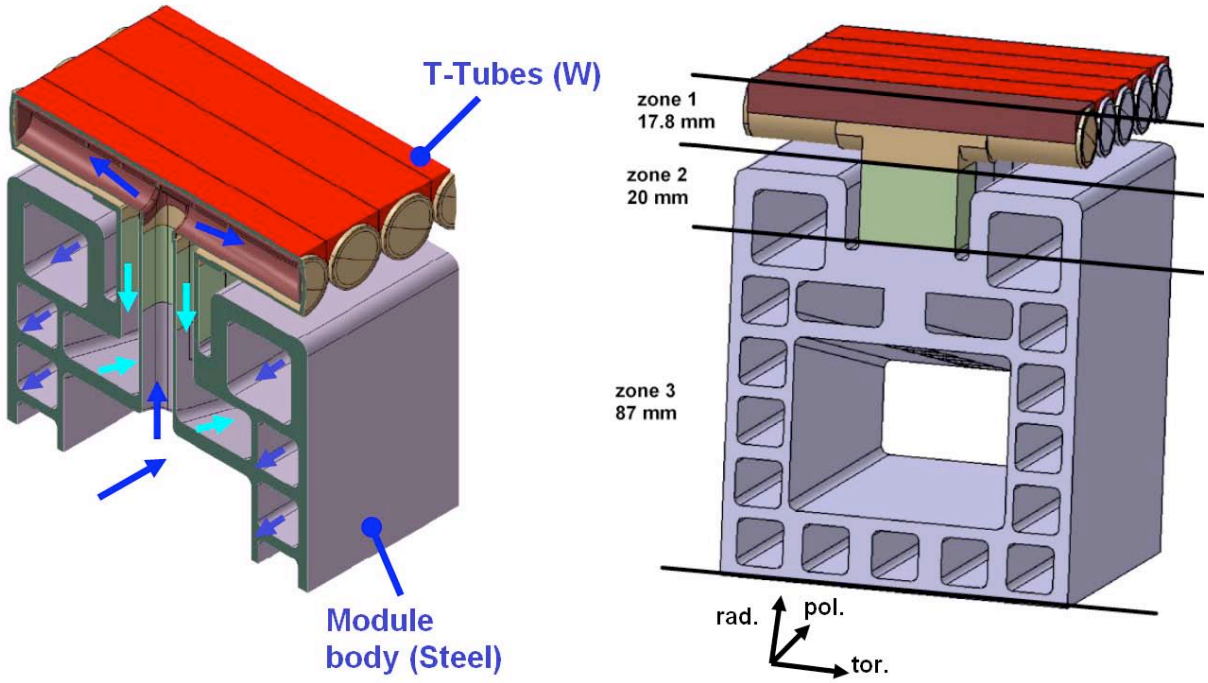

Fig. A3.2: Target and manifold design concept (detailed CAD model)

Appendix 4: Integration of the divertor targets

A4.1 Geometrical divertor target integration options

In general it was decided to consider the same cutting and re-welding option for the divertor tubes as used for the blanket connection tubes. This means, that the connection to the manifold, witch is located behind the shield is made by radial connection tubes, which pass through the shields. Cut-outs around the tubes are used to provide sufficient space for the welding and cutting tools to access the tubes. These cut outs are thought to be closed by use of inserts (possibly made of tungsten carbide). The tubes are concentric with inlet coolant being directed in the annular gap between inner and outer tube and the outlet coolant flow being directed through the inner tube. For details of this procedure see the description in section 3.1 of the main text. Note that previous to a final decision on the cutting and re-welding scheme the sufficiency of the shielding in the tube areas has to be analyzed carefully in every respect by use of 3D neutronic calculations.

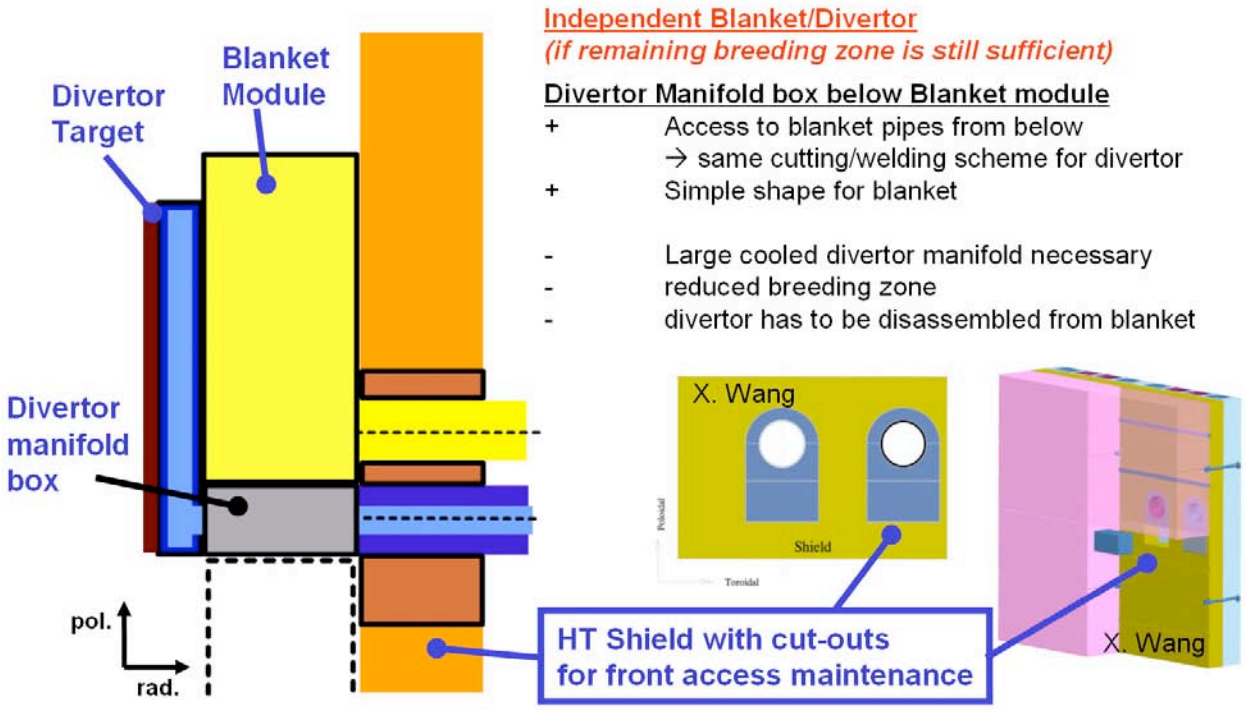

Fig. A4.1: Cutting & re-welding scheme applying cut-outs in the HT shields along with a divertor target in front of the blanket module and a box like divertor main manifold placed between two adjacent blanket boxes

As for tritium breeding self-sufficiency nearly the complete plasma facing interior area of the compact stellarator is needed to place breeding blankets, the divertor targets have to be placed in front of the blanket modules. From this it is evident that the divertor targets have to be

mechanically connected to the blanket modules. The divertor main manifolds have to be placed either between the blanket modules or partly or completely within the blanket modules. If the remaining breeding area is still sufficient cooled steel manifolds between the adjacent blanket modules could be realized. The resulting outer shape of the blanket modules and the divertor manifold box would be simple, but the inner cooling structure of the manifold box is relatively complicated and will cause some additional pressure drops. The according integration scheme is illustrated in fig. 4.1 along with a table showing the advantages and drawbacks.

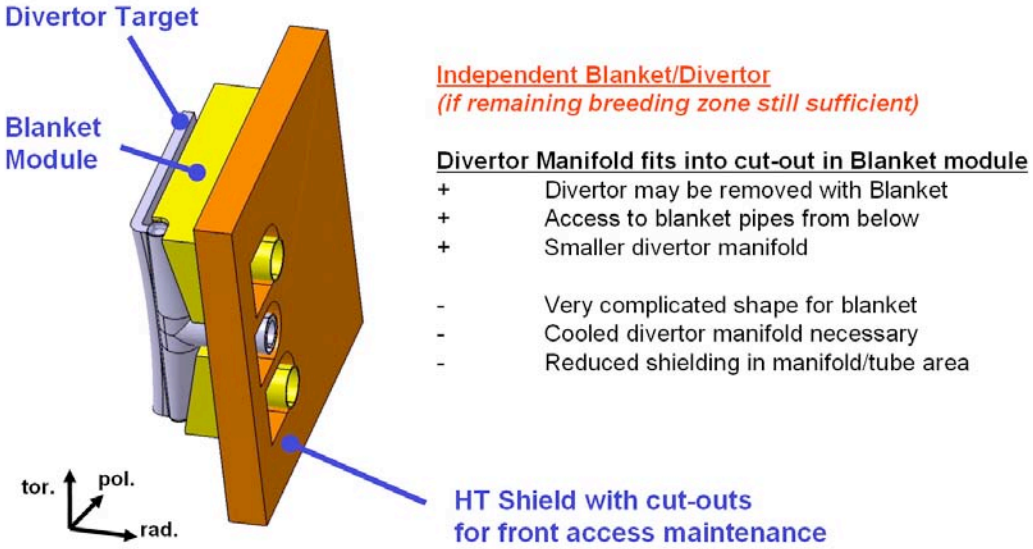

Fig. A4.2: Cutting & re-welding scheme applying cut-outs in the HT shields along with a divertor target in front of the blanket module and a tapered divertor main manifold placed in a cut-out within a blanket box

Alternative schemes applying tapered divertor main manifolds are shown in figs. A4.2 and A4.3 along with the corresponding advantages and drawbacks. Fig. A4.4 illustrates an alternative option with the blanket main manifold being integrated in the blanket main box. For the current dual coolant blanket design for the port maintenance approach the manifolds for the blanket (Helium coolant and the liquid metal manifolds) are placed within the blanket main boxes. These manifolds are designed as different layers of a cubic manifold at the lower backside of the blanket box. The divertor helium coolant manifold and collector can be inserted as two additional layers at the backside of the present blanket manifold. By this the existing side and back walls of the blanket box act also as walls for the divertor main manifold, reducing the total amount of necessary cooled steel structure. The divertor target manifolds (stripe like as shown in fig. A3.1 and A3.2) will penetrate the blanket box at its lower backside. As the temperature level of the divertor steel structure is higher than the blanket box temperature the resulting thermal stresses at the penetration area were considered carefully. As a result of this approach it can be concluded, that the stress levels can be drastically reduced, if gaps between the adjacent radial directed stripe-like divertor target modules are used to allow for the relative expansions between

the hot area of the stripe modules and the cold area of the stripe modules within the cooler blanket box.

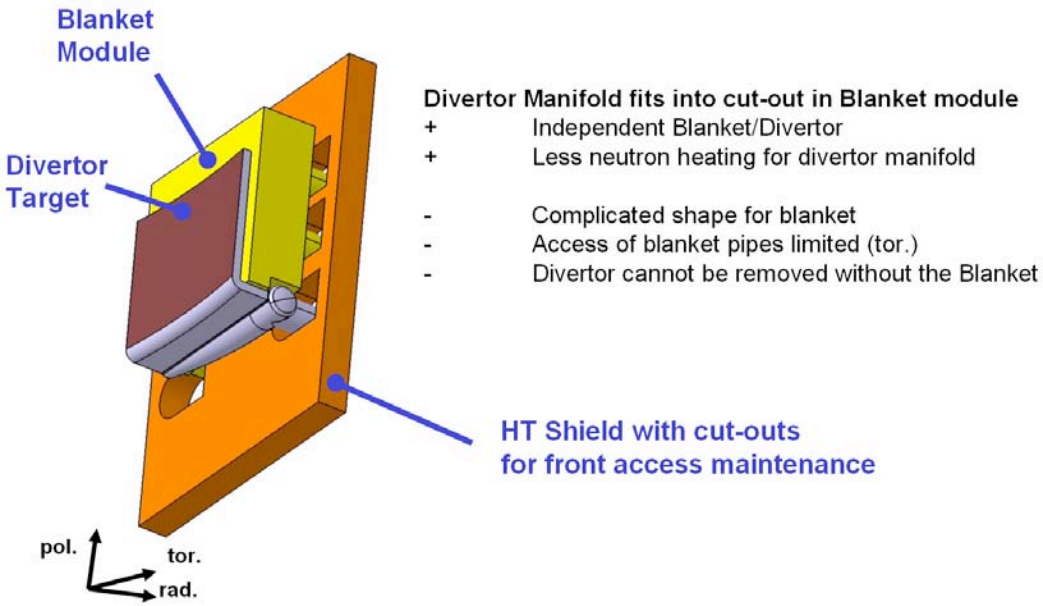

Fig. A4.3: Divertor target in front of the blanket module,
tapered divertor main manifold placed in a cut-out within a blanket box

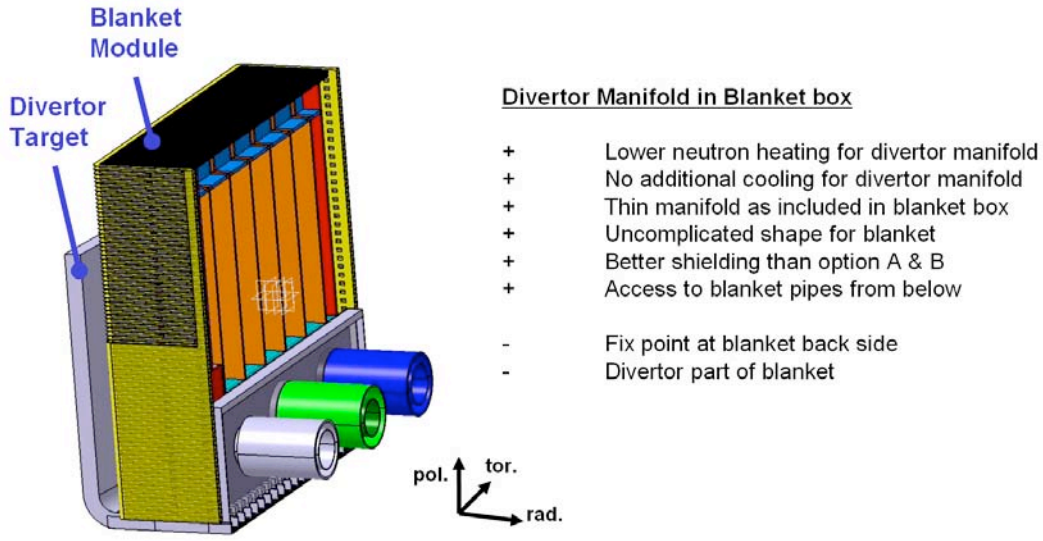

Fig. A4.4: Cutting & re-welding scheme applying cut-outs in the HT shields along with a divertor target in front of the blanket module and a tapered divertor main manifold placed in a cut-out within a blanket box

A4.2 Exemplary layout of the divertor targets

In the following a layout example is given for an assumed Gaussian heat flux distribution function along the target plate in poloidal direction and uniformity of the heat flux in toroidal direction (see fig. A4.5).

The main boundary conditions for the layout example are:

Maximum heat flux:	10	MW/m²
Averaged heat flux:	3	MW/m²
Inlet temperature	600	°C
Outlet temperature	≤ 700	°C
Helium pressure	10	MPa
Target plate length (poloidal)	1	m
Target plate width (toroidal)	2	m
Velocity in the main supply	75	m/s
Velocity in channels & manifolds	≤ 60	m/s

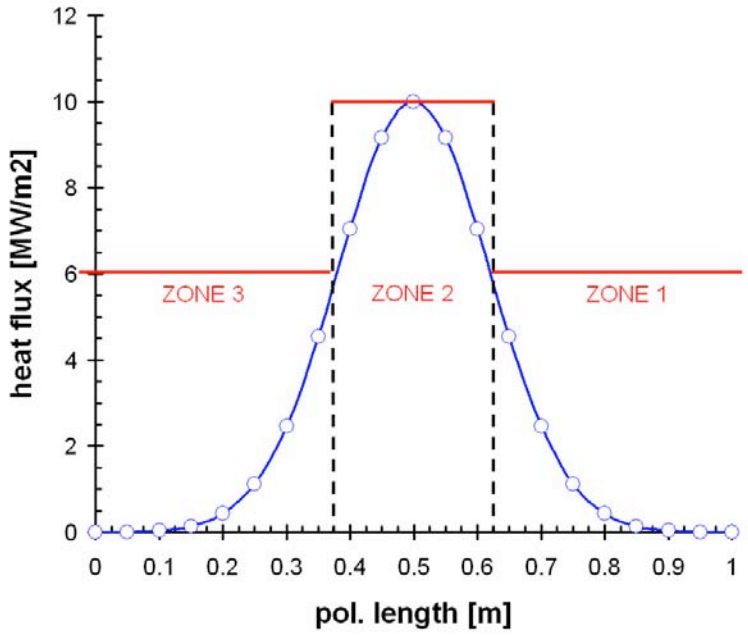

Fig. A4.5: Exemplary heat flux distribution function and target cooling zones

The target plate is divided into three cooling zones in poloidal direction, for each cooling zone stripe like parallel modules are foreseen. Between the cooling zones series connections are necessary (as indicated in fig. A3.1). In cooling zone 2 small cooling fingers with a tube diameter of 15 mm appropriate to handle heat fluxes up to 10 MW/m² will be used as described in section 3 of the main text (parameter of the T-tube heat exchange part layout are shown in table 1). The poloidal length of cooling zone 1 was chosen to be 0.25 m to reach the necessary mass flow per

target surface unit of 24 kg/(s m²) (table 1 in main text) along with a total heat up of the coolant shortly below 100 K. The total mass flow G_{target_plate} for the considered target width of 2 m (equals blanket width) is:

$$G_{target\_plate} = 24\frac{kg}{s\cdot m^2}\cdot 2m\cdot 0.25m = 12\frac{kg}{s}$$

This total target plate mass flow along with the averaged heat load of 3 MW/m² results in a total coolant heating ΔT_{target} of:

$$\Delta T_{target} = \frac{3\cdot 10^6 W\cdot s\cdot 2m\cdot 1m\cdot kg}{12kg\cdot m^2\cdot 5200W}K = 96K$$

The concentric connection tube for the main divertor can be dimensioned with the helium parameter, the flow velocity as given above and the ultimate tensile strength of 395 MPa assumed for the steel used for the outer supply tubes at 600°C. The inner diameter of the inner tube was set to 205 mm (flow velocity 73 m/s), the outer diameter is 225 mm. The inner diameter of the outer tube can be set to be 297 mm resulting in a flow velocity of 74 m/s, while the necessary wall thickness for the tube was calculated to be 14 mm finally leading to the outer tube outer diameter of 325 mm. From this the divertor supply tube is of the same size as the blanket supply tubes (liquid metal and helium) foreseen for the dual coolant blanket modules (blanket size: 2m x 2m).

The pressure drop in the concentric supply tubes was calculated as follows:

Absolute roughness of tube surface: K = 0.05 mm

Relative roughness: e = K/D = 0.05/205 = 2.44e-4

Reynolds number : Re = 2.36e6

Pressure loss coefficient:
$$\xi = \left(-2\log\left(\frac{2.51}{\mathrm{Re}\cdot\sqrt{\xi}} + \frac{e}{3.71}\right)\right)^{-2} \Rightarrow \xi = 0.0147$$

Pressure loss due to friction in main tube (length set to l = 20 m):

$$\Delta p_{friction\_main tube} = \xi\cdot\frac{l}{D}\cdot\frac{\rho}{2}\cdot w^2 = \frac{0.0147\cdot 20\cdot 5.22\cdot 73^2}{0.205\cdot 2}Pa = 2.0\cdot 10^4 Pa$$

For reasons of simplicity the total pressure drop due to friction of the concentric tube (inlet + outlet) was set to be twice the main tube pressure drop calculated above. The 90 degree turn for the inlet and outlet main connection to the divertor manifold was taken into account along with additional turns resulting in a total pressure drop due to direction changes of 1.55 e4 Pa. The total pressure drop for the concentric main supply tubes gets:

$$\Delta p_{total\_main tube} = \left(2\cdot 2.0\cdot 10^4 + 1.55\cdot 10^4\right)Pa = 5.55\cdot 10^4 Pa$$

Similarly the pressure drops for the target manifold channels were calculated. Results:

Pressure drop in small outer channels of the target manifolds (see fig. A3.2):

$$\Delta p_{TARGET\_small\_ChANNELS} = 4.88 \cdot 10^4 \, Pa$$

Pressure drop for the inner main channels in the target manifolds (see fig. A3.2):

$$\Delta p_{TARGET\_large\_ChANNELS} = 2.47 \cdot 10^4 \, Pa$$

Further on the pressure drop in the T-tubes was determined. The pressure drop in zone 2 is:

$$\Delta p_{T-tube\_zone2} = 1.19 \cdot 10^5 \, Pa$$

In zone 1 and 3 the maximum heat flux is below 6 MW/m² (see fig. 4.5). Using the scaling scheme presented in this report (section 2.2.1) the tubes can be scaled up with the scaling factor being the inverse of the heat flux ratio (6/10). Therefore, the T-tubes in zone 1 and 3 have an outer diameter of 25 mm (10/6 times 15 mm). The length of the T-tubes in zone 1 and 3 was set to be twice the length of the tubes in zone 2 to keep the divertor target manifold design simple. Note that the maximum thermal stress level is determined by the geometrical parameters in T-region and therefore the slightly higher scaling (10/5) of the tube's length in relation on the scaling of width, wall thickness and height (10/6) can be applied. The slot width for the cartridges in zone 1 and 3 (slot width b = 0.97 mm) was adjusted to obtain an averaged heat transfer coefficient of about 10,400 W/m²K at the inside of the tubes which is sufficient to handle heat fluxes up to 6 MW/m² without exceeding the defined material temperature limits. As a result the pressure drop in zone 1 (pressure drop in zone 3 is the same) was calculated to be:

$$\Delta p_{T-tube\_zone1} = 4.53 \cdot 10^4 \, Pa$$

The total pressure drop for the divertor including the main supply tubes can be calculated to be:

$$\Delta p_{divertor} = \Delta p_{total\_main} + \Delta p_{small\_Ch.} + \Delta p_{large\_Ch.} + \Delta p_{T-tube\_zone2} + 2 \cdot \Delta p_{T-tube\_zone1} = 3.38 \cdot 10^5 \, Pa$$

The necessary circulation power (isentropic blower power) for the divertor at a temperature of about 570°C can be determined:

$$P_{circulation\_target plate} = \frac{\Delta p_{divertorn} \cdot G_{target plate}}{\rho} = 0.71 MW$$

The resulting relative circulation power (volumetric heating neglected):

$$\frac{P_{circulation\_target plate}}{\dot{q}_{target plate} \cdot A_{target plate}} = \frac{0.71 MW}{3 \, {}^{MW}/_{m^2} \cdot 2 m^2} = 11.8\%$$

Assuming a total heat load of <u>200 MW</u> for the ARIES CS divertor the total isentropic blower power can be calculated:

$$P_{circulation\_divertor} = 11.8\% \cdot 200 MW = 23.6 MW$$

Note: The final layout of the ARIES CS divertor may become much more complicated, if local heat flux peaking and non-uniformities in toroidal direction occur. Both effects tend to result in increased circulation power demand compared to the current layout example.